JGR Atmospheres

RESEARCH ARTICLE
10.1029/2018JD030151

East Asian Monsoon as a Modulator of U.S. Great Plains Heat Waves

Hosmay Lopez[1,2], Sang-Ki Lee[2], Shenfu Dong[2], Gustavo Goni[2], Ben Kirtman[1], Robert Atlas[2], and Arun Kumar[3]

[1]Cooperative Institute for Marine and Atmospheric Studies, University of Miami, Miami, FL, USA, [2]Atlantic Oceanographic and Meteorological Laboratory, NOAA, Miami, FL, USA, [3]Climate Prediction Center, NOAA, College Park, MD, USA

Key Points:
- The influence of the East Asian Monsoon (EAM) on the summer climate of the Great Plains of the United States is investigated
- The EAM forces an upper-level ridge over the Great Plains of the United States, increasing temperature and drought over that region in boreal summer
- The amplitude and frequency of occurrence of heat waves increases as a result of the reduced precipitation and stagnant circulation

Correspondence to:
H. Lopez,
hlopez@rsmas.miami.edu

Citation:
Lopez, H., Lee, S.-K., Dong, S., Goni, G., Kirtman, B., Atlas, R., & Kumar, A. (2019). East Asian Monsoon as a modulator of U.S. Great Plains heat waves. *Journal of Geophysical Research: Atmospheres*, *124*. https://doi.org/10.1029/2018JD030151

Received 10 DEC 2018
Accepted 12 MAY 2019
Accepted article online 30 MAY 2019

Author Contributions:
Conceptualization: Hosmay Lopez, Sang-Ki Lee, Shenfu Dong, Ben Kirtman, Robert Atlas, Arun Kumar
Formal analysis: Hosmay Lopez
Investigation: Hosmay Lopez
Methodology: Hosmay Lopez, Sang-Ki Lee, Shenfu Dong, Gustavo Goni, Ben Kirtman, Robert Atlas, Arun Kumar
Resources: Hosmay Lopez
Supervision: Sang-Ki Lee, Shenfu Dong, Gustavo Goni, Ben Kirtman, Robert Atlas, Arun Kumar
Validation: Hosmay Lopez, Shenfu Dong
Visualization: Hosmay Lopez
Writing - original draft: Hosmay Lopez, Sang-Ki Lee, Ben Kirtman, Robert Atlas, Arun Kumar
Writing – review & editing: Hosmay Lopez, Sang-Ki Lee, Shenfu Dong, Gustavo Goni, Ben Kirtman, Robert Atlas, Arun Kumar

Abstract Heat waves are the leading weather-related cause of death in the United States, with the most recent examples occurring in the summers of 2011 and 2012 over the Great Plains. These events are unusual and largely unpredictable beyond the synoptic timescale. Their number and severity have increased and are projected to continue to increase, prompting the need to identify the physical processes that modulate heat waves and, consequently, can lead to improved prediction and future projection. Our results based on observations and model simulations suggest that convective latent heat release from the East Asian Monsoon enhances the likelihood of droughts and heat waves over the United States through an equivalent barotropic wave train along the subtropical jet stream, promoting an anticyclonic circulation pattern over the Great Plains. This anticyclone serves as a blocking pattern for transient synoptic-scale systems and is supportive of persistent drought and clear sky conditions, promoting high temperatures and heat waves.

1. Introduction

Heat waves are large-scale and persistent extreme warm temperature events that are responsible for the most weather-related cause of death in the United States. Specifically, the U.S. Great Plains has historically experienced devastating heat waves with high human mortality and economic impacts. The most recent extreme events occurred during the consecutive summers of 2011 and 2012, with 206 and 155 fatalities (well above the 10-year average of 97 deaths) according to the U.S. Natural Hazard statistics. During the summer of 2011, places like Oklahoma City, OK, saw over 40 days of maximum temperature exceeding 100 °F (37.8 °C), as well as both maximum and minimum temperatures above the 95th percentile (Figure 1a). Similarly, the 2012 heat wave broke several all-time temperature records, reaching 111 °F (43.9 °C) in Dodge City, KS, on 27 June 2012 (Figure 1b).

Heat waves are linked to specific weather patterns and boundary conditions that involve, for example, atmospheric circulation, precipitation deficits, sea surface temperatures, and soil moisture content (Atlas et al., 1993). Atmospheric high-amplitude planetary circulation patterns, such as lingering blocking patterns, are linked with extreme heat wave events (Petoukhov et al., 2013). The climate community has been increasingly dedicated to understanding and to eventually predicting heat waves beyond the 10-day synoptic forecast range. For example, Sutton and Hodson (2005) identified that sea surface temperature variability could significantly influence the summertime atmospheric circulation pattern and climate anomalies over North America and Europe, including extremes. Trenberth and Fasullo (2012) argued that a global perspective is necessary in order to understand factors that can potentially influence these extreme events. Teng et al. (2013) found potential source of predictability of heat waves on subseasonal timescales. They found that a specific midlatitude atmospheric circulation pattern precedes heat waves over the United States by 15–20 days, well beyond the traditional synoptic forecast range.

Seasonal predictability of surface air temperature and precipitation over the United States is mostly driven by the El Niño-Southern Oscillation (ENSO) state during the winter and early spring months (Infanti & Kirtman, 2016; Kam et al., 2014; Lee et al., 2018). Other teleconnection patterns, such as the Pacific North American pattern and the East Pacific wave-train, have been shown to be useful predictors of upper-atmosphere high pressure (i.e., ridging) that accompanies western U.S. droughts, potentially leading to heat extremes (Lin et al., 2017; Piao et al., 2016). Unlike for the winter, predictability of large-scale atmospheric teleconnection patterns during the summer are difficult largely because the background state

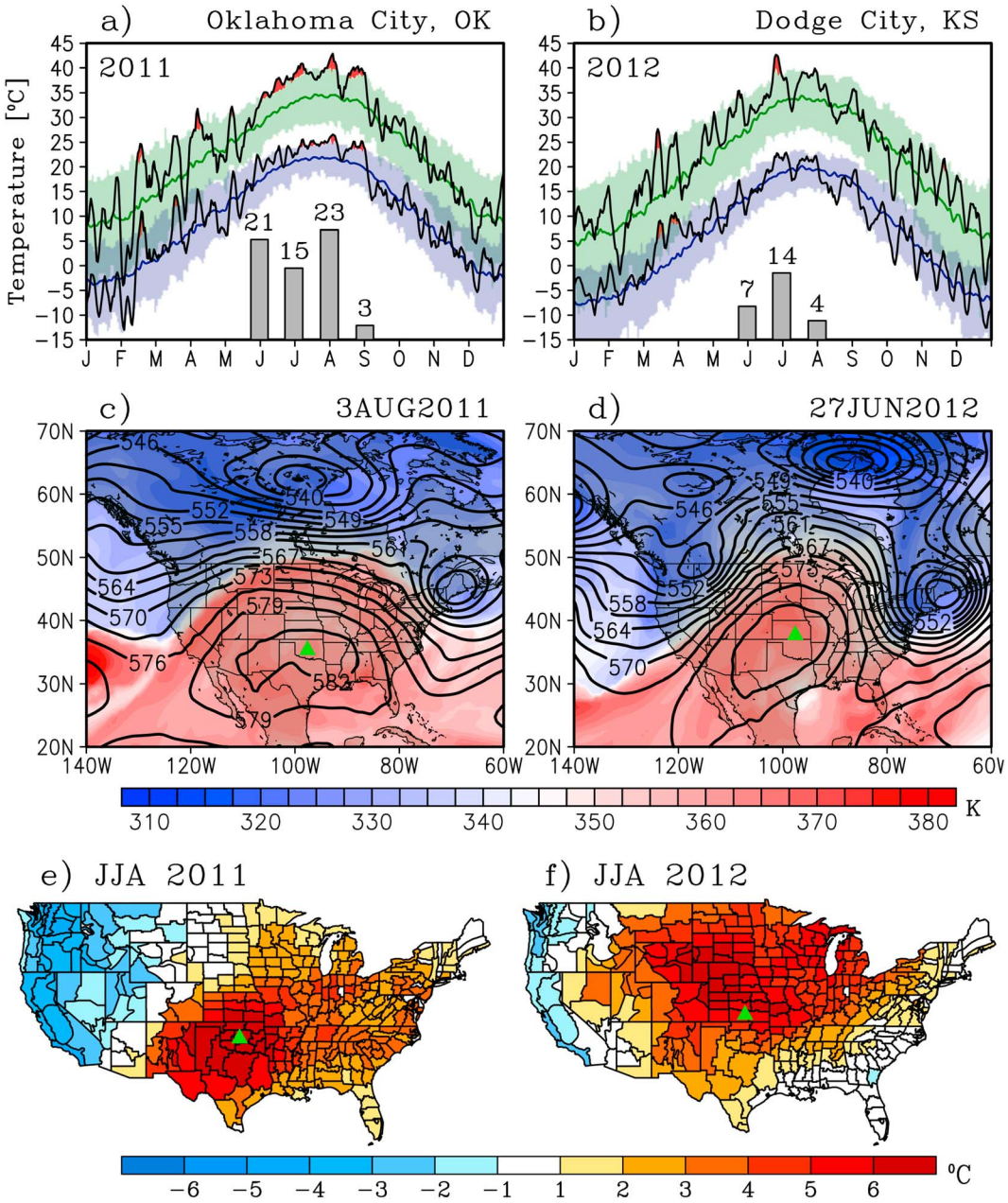

Figure 1. Daily maximum and minimum temperature for (a) 2011 Oklahoma City, OK, and (b) 2012 Dodge City, KS. The 95th percentile is indicated by the green (purple) shading for the maximum (minimum) temperature. Temperatures exceeding the 95th percentile are shaded red. The gray bar plot and numerical values indicate the number of days for each month exceeding the Excess Heat Factor (EHF) threshold. (c and d) Potential temperature at the tropopause (shading) and 500-hPa geopotential height during the 2011 and 2012 heat waves, respectively. The location of the stations is marked by the green triangle. (e and f) June-July-August surface temperature anomaly (°C) during the 2011 and 2012 Great Plains heat waves.

is relatively weak and too far from the tropics, where such teleconnection patterns are typically forced (e.g., Lee et al., 2009).

La Niña conditions were present during the 2011 and 2012; however, several studies suggest that internal atmospheric variability rather than remote sea surface temperature forcing was the dominant driver of the extreme droughts and heat waves of 2011 and 2012 (Hoerling et al., 2014; Seager et al., 2014). The 2011 and 2012 heat waves were accompanied by high amplitude positive high anomalies and potential temperature as high as 370 K at the tropopause, following an omega-blocking pattern (Figures 1c and 1d). Vertical profiles for Oklahoma City on 3 August 2011 and from Dodge City on 27 June 2012 (Figure 2)

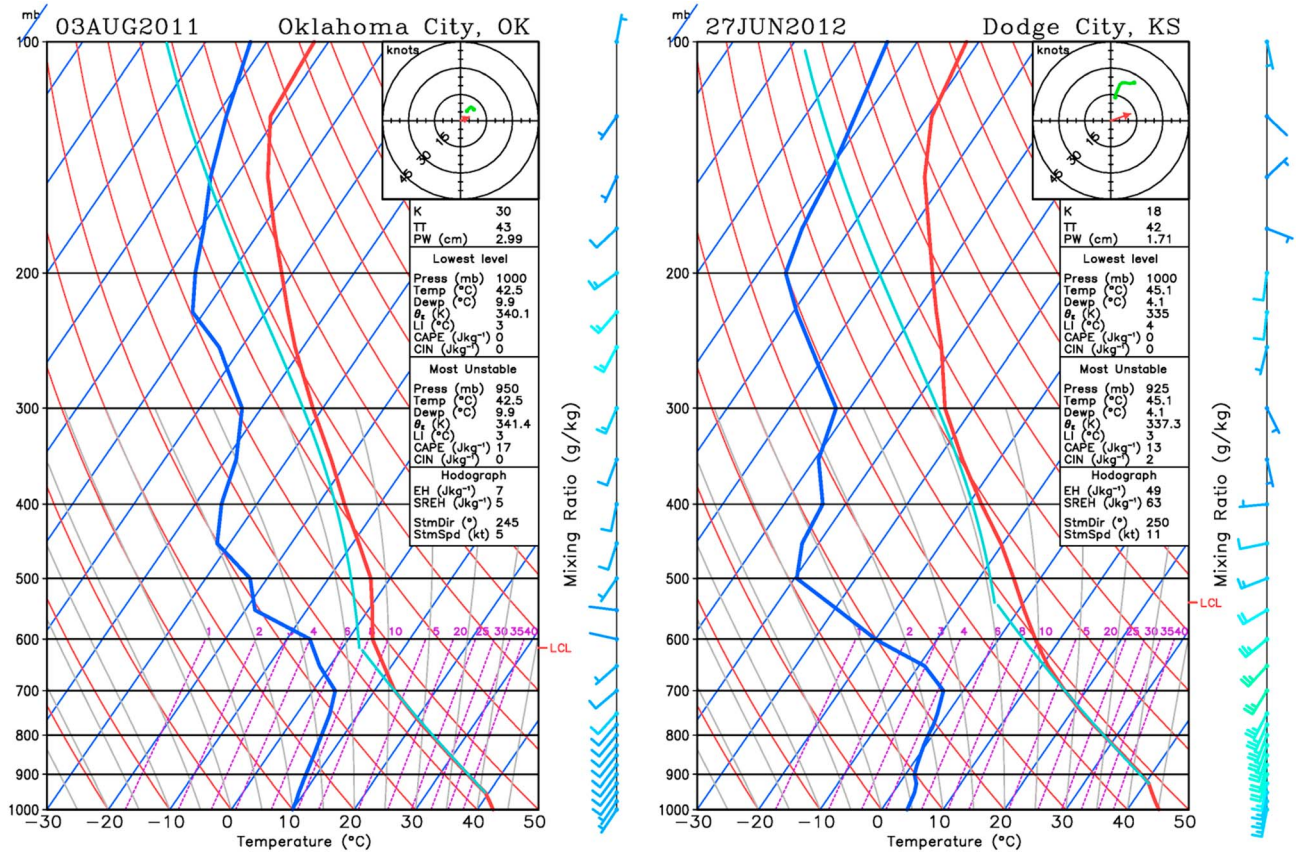

Figure 2. Vertical atmospheric profiles for 3 August 2011 over Oklahoma City, OK (left), and 27 June 2012 over Dodge City, KS (right). The profiles are plotted on a skew*T*-log*P* thermodynamic diagram. The vertical axis is the pressure (hPa), the skewed thin blue axis denoted temperature (Celsius), the thin red lines represent dry adiabats, and the thin gray lines denote moist adiabats. The vertical profile of environmental temperature, dew point, and wind speed and direction are denoted by the thick red, thick blue, and wind bard. A surface-based parcel profile is shown by light blue for reference. Several stability criteria are given in the table.

show a well-mixed lower troposphere, with a deep dry layer of constant potential temperature and mixing ratios from the surface up to about 700 mb, indicating strong turbulent heat and moisture fluxes associated with enhanced surface heating from prolonged clear sky conditions. Both profiles also show a marked decrease in dew point temperature above 600 mb, indicative of deep subsidence associated with the high-pressure dome as well as weak wind speed and vertical wind shear. These patterns were very persistent throughout the 2011 and 2012 summers, resulting in June-July-August (JJA) temperature anomalies exceeding 5 °C for most of the central United States (Figures 1e and 1f). Wang et al. (2014) showed that these upper-tropospheric high anomalies were linked to stationary Rossby waves and supported by transient eddies and were the lead cause of these extreme heat waves.

On top of the difficulties in predicting heat waves beyond a few days and their devastating impact on society, the number and severity of these extreme events have been increasing in recent decades (Meehl & Tebaldi, 2004) and are projected to continue increasing into the 21st century with contributions from anthropogenic (i.e., human influence) forcing. Future projections of heat extremes and the role of anthropogenic forcing on its modulation are still not well understood, where a consensus has not been reached regarding the mechanisms linking extreme events to anthropogenic forcing (Palmer, 2013; Shepherd, 2014; Teng et al., 2016). Given these findings, there is large uncertainty in future projection of heat waves over the United States. For example, Lopez et al. (2018) showed that anthropogenic forcing will dominate the occurrence of heat waves over the western United States and Great Lakes region, whereas the presence of large natural variability that governs heat wave occurrence over the Great Plains adds uncertainty in their future projections. They found a strong negative correlation between the projected changes in the Great Plains low-level jet amplitude and the projected changes in the number of heat wave days among CMIP5 models, identifying a potential large-scale pattern that could aid in heat wave predictions. This result calls for the need to

identify potential remote linkages of these extreme events over the Great Plains that would aid in their prediction and understanding of future projections.

While summer mean atmospheric circulation is relatively weak, hence limiting large-scale teleconnections, the extra-tropical nature of the East Asian Monsoon (EAM) and its proximity to the mean midlatitude storm track allow for heating anomalies to remotely influence circulation. In a search for remote influences that can modulate summer climate over the United States, Wang et al. (2001) showed that diabatic heating associated with the EAM and its connection with summer climate over the United States may be a possible candidate. Zhu and Li (2016) proposed an Asian-North American teleconnection pattern in boreal summer linking East Asian subtropical monsoon rainfall and continental U.S. rainfall. More recently, Zhu and Li (2018) showed that a northward shift of the EAM enhances U.S. summer rainfall variability. The EAM is characterized by a boreal summer precipitation maximum over East Asia and is responsible for most of the annual total rainfall in eastern China, the Korean peninsula, and Japan (Sample & Xie, 2010). The EAM is located on the western edge of the North Pacific Subtropical High and is associated with significant low-level moisture transport from the southwesterly wind (Kodama, 1992). Low-level moisture convergence and cumulus deep convection is responsible for the midtropospheric diabatic heating and the circulation changes over the EAM (Sample & Xie, 2009).

Given these observational evidences that the EAM variability can potentially force U.S. summer climate (e.g., Wang et al., 2001; Zhu & Li, 2018), we explore the influence of diabatic heating over the EAM as a potential modulator of extreme heat waves over the Great Plains, such as those events in 2011 and 2012. Our hypothesis is that midtropospheric heating due to deep convection from the EAM forces a stationary wave pattern across the North Pacific, setting up the stage for increased likelihood for atmospheric "blocking" events and heat waves over the Great Plains. The remaining of this paper is as follows: section 2 describes the data sets, models, and experiments used, section 3 looks at the typical U.S. Great Plains heat wave patterns and associated circulation, section 4 touches on the physical mechanisms for EAM teleconnections, section 5 investigates the modulation of heat extremes by the EAM, and further discussion and conclusions are presented in section 6.

2. Data, Models, and Methods

The extreme temperature and heat wave events, as well as the associated large-scale atmospheric circulation, are analyzed using daily mean near-surface air temperatures from the European Center for Medium-Range Weather Forecast Twentieth Century Reanalysis (ERA-20C; Poli et al., 2016). We choose the ERA-20C in order to be consistent with Lopez et al. (2018) as their study served as the main motivation as well as the basis for the analysis presented here. Also, ERA-20C provides a long record (1900–2010) of daily near-surface temperature that is reliable over North America for the computation of heat waves. The computation of heat waves relies on the information of the tails of the distribution, thus requiring long records to extract meaningful statistics. Daily and monthly mean precipitation data comes from the Global Precipitation Climatology Project (Huffman et al., 1997). We also use observational estimates of vertical profiles of atmospheric heating rates from the Japanese 25-year Reanalysis of the Japan Meteorological Agency (Onogi et al., 2007) in order to describe the four-dimensional diabatic (i.e., convective plus large-scale) heating rates associated with the EAM precipitation.

2.1. Models

The rareness of extreme events, the short observational record, and the relative noisiness of midlatitude summer atmospheric variability all contribute to making the study of heat waves difficult. Therefore, in addition to the reanalysis data, we also use a long preindustrial simulation of the Community Earth System Model (CESM1) Large Ensemble Simulation (Kay et al., 2015) from the National Center for Atmosphere Research. This Earth system model consists of atmosphere, land, ocean, glaciers, and sea ice components, all linked by a flux coupler. The atmospheric component is the Community Atmosphere Model version 5. It has 30 vertical levels with horizontal resolution of 1.25° longitude by 0.94° latitude. The ocean model component uses the Parallel Ocean Program version 2. It has a 1° horizontal resolution with 60 vertical levels. Here we analyze 1,100 years of preindustrial simulation with constant atmospheric chemical composition based on the year 1850. This preindustrial simulation serves as the basis for the analysis of heat waves and their natural variability in the absence of external (i.e., human-induced) forcing.

We also make use of a linear baroclinic model (LBM; Watanabe & Kimoto, 2000) in order to assess atmospheric teleconnection patterns associated with diabatic heating from the monsoons and their relationship to heat waves over the United States. This LBM is a primitive equation model linearized about a basic state, usually taken as monthly, seasonal, or annual mean climatology. The aim here is to understand complex atmospheric processes in a simplified way by removing their nonlinear aspects. For this study, the model is run at a horizontal resolution of T42 (roughly 2.8° latitude) and 11 vertical levels in a sigma (i.e., surface-pressure normalized) coordinate system. The LBM is forced by prescribing diabatic heating rate profiles as those observed for the EAM. More details are provided in section 4.

2.2. EAM Index

The EAM index is defined by area-averaging precipitation over East Asia where the June-July-August-September minus December-January-February-March Annual precipitation range is greater than 2 mm/day and the local summer precipitation exceeds 55% of the total annual precipitation, following Wang et al. (2012). Since reliable precipitation observations only date back to 1979 and heat waves are rare by definition, we extended the EAM index using shear vorticity anomalies in order to increase the observed sample size, following Wang et al. (2008). The reconstructed EAM index is defined as U_{850} in (22.5–32.5°N, 110–140°E) minus U_{850} in 5–15°N, 90–130°E, where U_{850} is the zonal wind at 850 hPa.

2.3. Heat Wave Index

The definition of heat waves proposed here is based on clustering warm extreme daily mean temperature that covers each summer from 1 June to 30 August (i.e., June-July-August; JJA) over the United States following Lopez et al. (2018). The clustering of heat waves allows us to separately assess their dependence on large-scale dynamics. This clustering technique provides the most common spatial pattern of heat waves as well as a time series of the number of heat wave days associated with each cluster and their amplitude.

3. Great Plains Heat Waves

Lopez et al. (2018) identified four main clusters over the United States, but here we only concentrate on the cluster affecting the Southern Great Plains (Figures 3a and 3c). This region was chosen because future projections of heat waves are uncertain due to very large natural variability there, calling for the need to identify potential natural causes for these events (Lopez et al., 2018). Both observational estimates and CESM show a large-scale high-amplitude temperature anomaly pattern extending for most of the Great Plains, which are very similar to the observed temperature anomalies during the 2011 and 2012 heat waves (Figures 1e and 1f). Note that the model is able to capture this pattern both in the spatial distribution and amplitude (Figure 3c). Figures 3b and 3d show the composite of 200-hPa streamfunction (color) and Rossby wave flux (vector) associated with Great Plains heat waves. The Rossby wave flux is quantified based on the Plumb (1985) formulation in an attempt to diagnose the propagation of stationary wave energy on a zonally asymmetric flow field. Observational estimates and CESM depict very similar wave trains across the Pacific Ocean with upper level ridging (i.e., anticyclonic circulation) over the Great Plains. This high-pressure dome is equivalent barotropic and very characteristic during heat waves. Unlike winter teleconnection patterns, summer atmosphere is less prone to teleconnections from remote forcing due to the weaker background flow and reduced synoptic variability over land (Schneider et al., 2014; Screen, 2014). The weaker background state calls for a weaker barotropic/baroclinic forcing of these Rossby waves, given that these waves cannot extract sufficient energy from the mean flow, limiting their wave source.

Here we investigate potential sources for these teleconnection patterns. For this purpose, the Rossby wave source is diagnosed as defined in Sardeshmukh and Hoskins (1988) and Kirtman et al. (2001). The Rossby wave source is a combination of vorticity advection by the divergent wind $-\boldsymbol{V}_\chi \cdot (\nabla\zeta)$ and vortex stretching by the divergent wind $-\zeta\nabla \cdot \boldsymbol{V}_\chi$, where ζ is vorticity and $\boldsymbol{V}_\chi$ is the divergent wind component. We hypothesize that upper level divergence associated with diabatic heating from an active summer monsoon system may initiate a Rossby wave source and hence force a stationary teleconnection pattern as shown in Figures 3b and 3d.

There is an upward propagation of Rossby wave flux (Figure 4a) and strong anticyclonic Rossby wave source over Japan and East Asia in boreal summer (Figure 4b), which becomes stronger at upper levels around 300–200h Pa. Coincidently, this is a region of strong precipitation (Figure 5a) and zonal wind associated with the

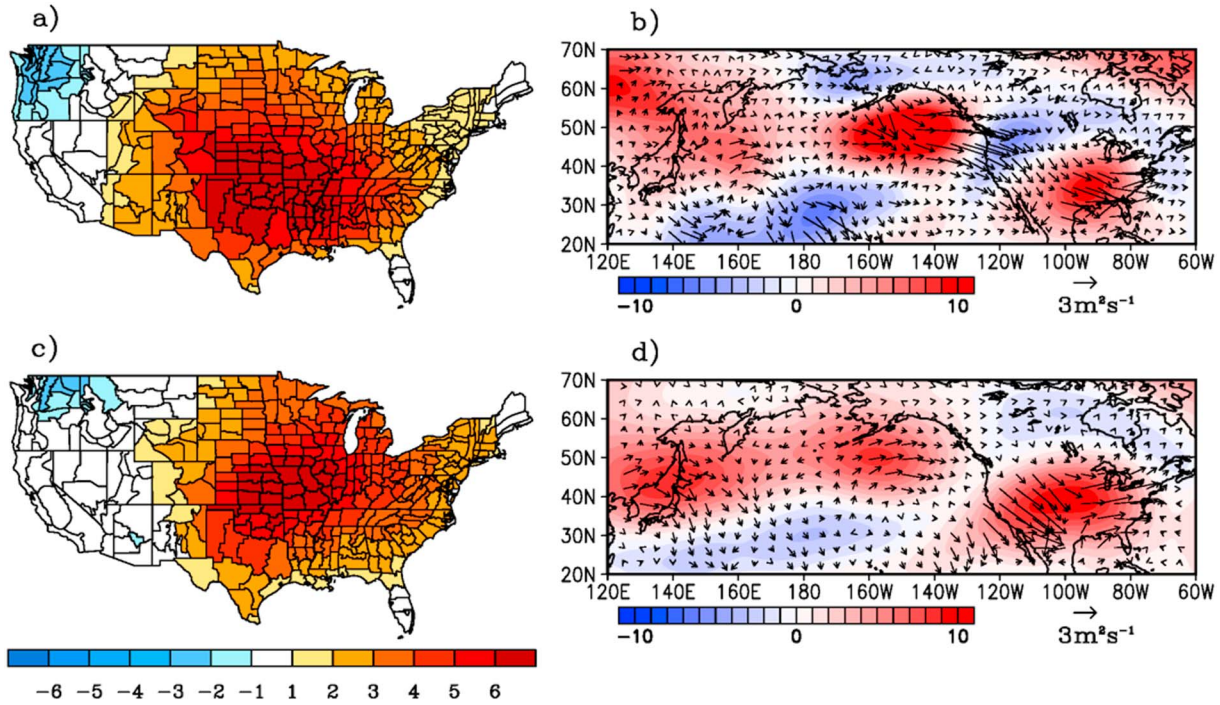

Figure 3. (a) Composite of observed surface temperature anomaly (°C) during Great Plains heat waves and (b) 200-mb streamfunction (color) and stationary Rossby wave flux (vector). (c and d) Same as (a) and (b) but for modeled heat wave events from CESM1.

subtropical jet (Figures 5b, 5c, and 5e) and midlevel diabatic heating associated with the EAM (Figure 5). This midlevel heating profile is responsible for a positive tendency in geopotential heights at upper levels as will be shown later and consistent with the anticyclonic wave source (Figure 4). Note also that the diabatic heating associated with the EAM is collocated under the right-entrance region of the jet streak (Figure 5b), reinforcing ascent. The term jet streak is widely used to signal a local wind speed maximum imbedded in the jet stream circulation. This theory is often themed as the jet-streak four-quadrant theory, which states, and by quasi-geostrophic assumptions, that forced ascending motion should be expected on the right-entrance and left-exit regions due to differential vorticity advection becoming more cyclonic with height (Bluestein, 1993; Namias & Clapp, 1949). Also note that the maximum heating occurs over the location of maximum rainfall (Figure 5a) as expected given that this precipitation is, for the most part, convectively driven. The double maximum heating in the longitudinal sense at 115°E and 130°E (Figure 5c) corresponds to the Meiyu-Baiu system (i.e., EAM) as discussed in Sampe & Xie, 2010). Also note that the main ascent occurs on the right entrance region of the "jet streak," or around 30°N and 130°E (Figure 5e), consistent with the main precipitation region.

Unlike for wintertime, tropical diabatic heating during summer cannot force extratropical teleconnection patterns due to the weak background state. Weak meridional vorticity and temperature gradients limit the potential for teleconnection patterns, decoupling the tropics from the extratropics in terma of teleconnections. The case for the EAM is different as it is the only monsoon system that reaches into the extratropics. In fact, the diabatic heating from the EAM is collocated near the climatological jet stream over Eastern Asia (Figure 5b). But since the EAM heating is near a region of strong ageostrophic forcing, which promotes rising motion, the EAM can readily force these Rossby waves along the storm track. This is consistent with the findings of Zhu and Li (2016) relating winter and summer teleconnection patterns.

4. LBM Experiment

To investigate if diabatic heating associated with the EAM can force teleconnection patterns similar to those associated with Great Plains heat waves (Figure 3), the LBM is forced with the observed EAM heating profile obtained from the Japanese 25-year Reanalysis as shown in Figure 5. These heating anomalies are prescribed

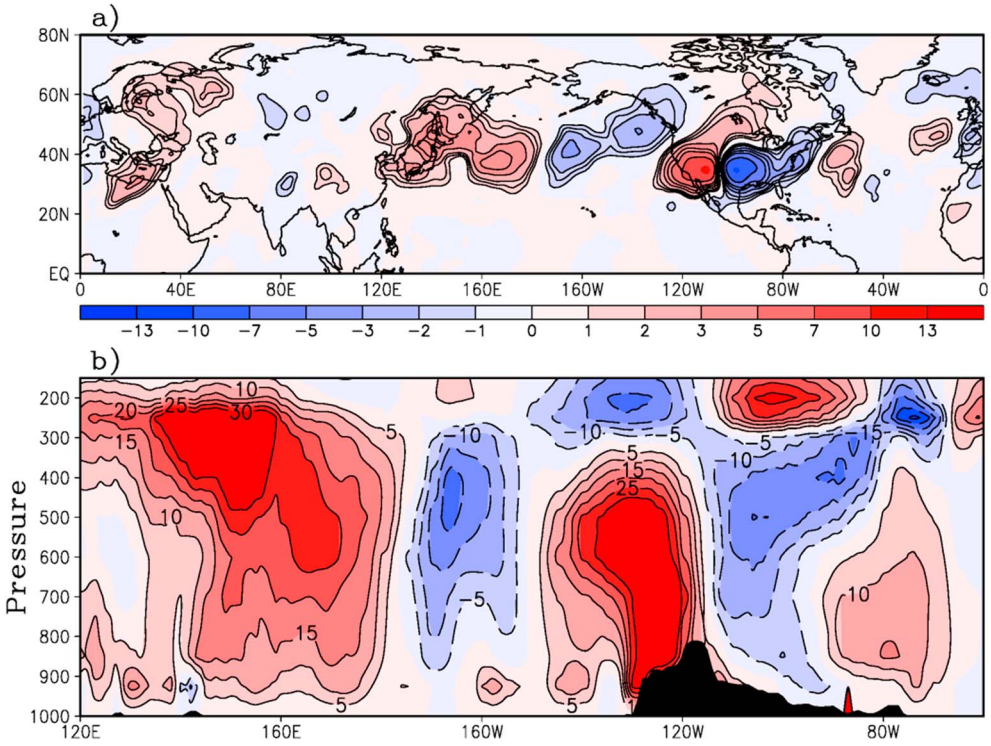

Figure 4. (a) Vertical component of the Rossby wave flux at 500 hPa (10^{-3} m^2/s). (b) Cross section of the Rossby wave source across the Pacific Ocean from 120°E and 35°N to 60°W and 35°N. Here anticyclonic (cyclonic) Rossby wave source is depicted by positive (negative) contour, respectively. Contour interval is 5×10^{-12} s^{-2}.

as heating rate and comprise of two terms: convective and large-scale condensation heating rate. Anomalies are defined here by the differences in heating rates between strong and weak EAM summers. For this experiment, the LBM is linearized about the zonally varying JJA basic state in order to allow for wave-wave interaction. We choose to diagnose the steady-state solution using the matrix inversion technique (Hoskins & Karoly, 1981; Watanabe & Kimoto, 2000) as it provides a simpler depiction of stationary teleconnection patterns than the traditional time-integration transient response.

Figure 6a shows the 200-hPa streamfunction steady response from the LBM. The response comprises of three major anticyclonic circulations, one centered over the EAM heating anomaly and directly driven by the mid-level heating profile, another over the Aleutian Low region, and the other over the Great Plains of the United States. The LBM response to the EAM forcing is remarkably similar to the teleconnection pattern associated with Great Plains heat waves as shown in Figures 3b (observed, pattern correlation of 0.62) and 3d (CESM, pattern correlation of 0.66). This is supportive of our hypothesis that the EAM could serve as a potential predictor of heat waves over the United States. To illustrate the importance of the climatological fields in generating teleconnections, we repeated the model experiment by forcing the LBM with the same diabatic heating anomaly, but the background state is changed to that of June, July, and August separately (Figures 5b, 5c, and 5d). Note that the 200-hPa zonal wind (green contour) weakens as we progress from June to August. With this, the teleconnection pattern as well as the blocking anticyclone over North America is also degraded. This is a direct result of weaker background state flow, leading to weaker forcing terms for stationary Rossby waves, which will be discussed in more details next. But overall, the wavenumber-3 teleconnection pattern is consistent throughout the summer months.

Physical mechanisms driving the stationary wave response shown in Figure 6 are investigated by diagnosing the quasigeostrophic height tendency. Here χ denotes the rate of change in geopotential height (i.e., increase in height when positive), $\boldsymbol{v}$ is the horizontal wind vector, θ represents the potential temperature, Q is the anomalous diabatic heating, f is the Coriolis parameter, σ is the mean static stability, β denotes the meridional variation of f, R is the ideal gas constant, c_p and c_v are specific heat of dry air at constant pressure and

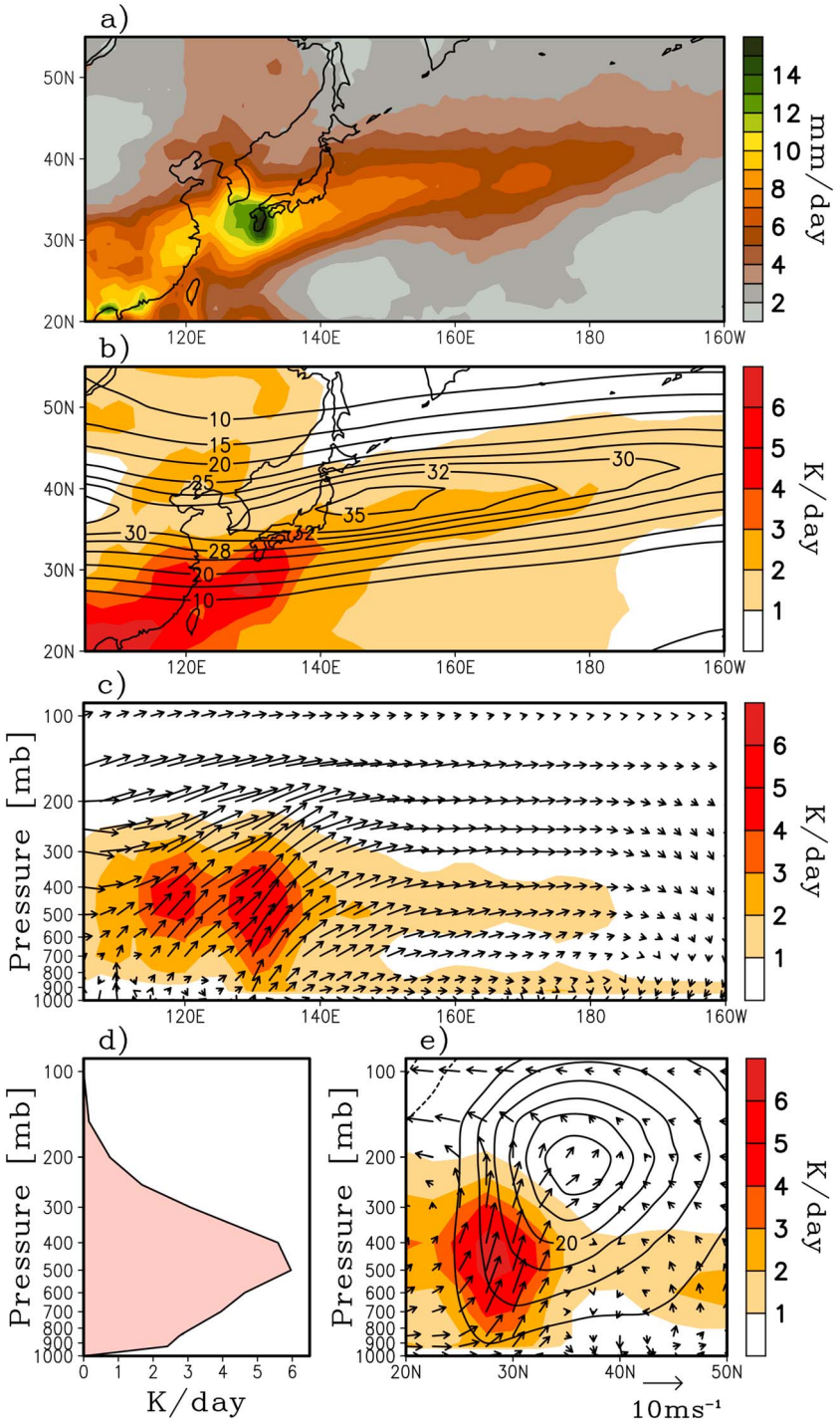

Figure 5. (a) June-July-August (JJA) mean precipitation over the East Asian Monsoon region. (b) JJA mean 250-hPa zonal wind (m/s, contour) and heating rate anomaly as prescribed in the linear baroclinic model (LBM; K/day, color). (c) Longitude-height cross section of heating rate along 30°N (color) and zonal and vertical wind (vector). (d) Vertical profile of heating rate centered at 130°E and 30°N. (e) Latitude-height cross section at 130°E of heating rate (color), zonal wind (contour, m/s), and meridional and vertical wind (vector). The heating rate anomaly shown in panels (b–e) is prescribed as forcing of the LBM experiment.

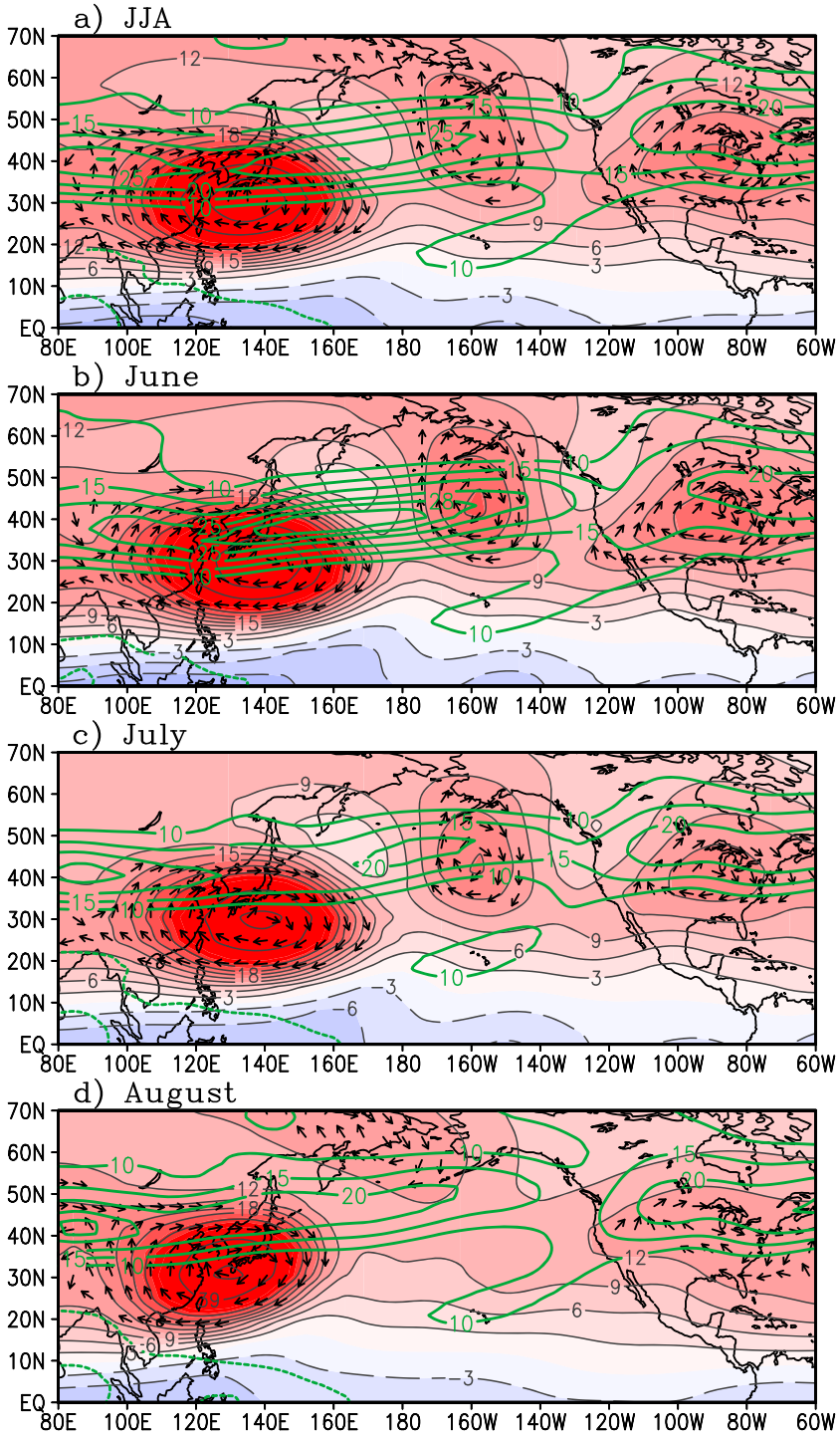

Figure 6. Steady-state linear baroclinic model response depicted by the 200-hPa streamfunction (color, contour interval 3 $\times 10^6$ s^{-1}) and rotational wind (vector) to the heating profile associated with the East Asian Monsoon shown in Figure 5. The background state is from (a) June-July-August (JJA), (b) June, (c) July, and (d) August. Different background states were chosen in order to illustrate the importance of subseasonality on teleconnection.

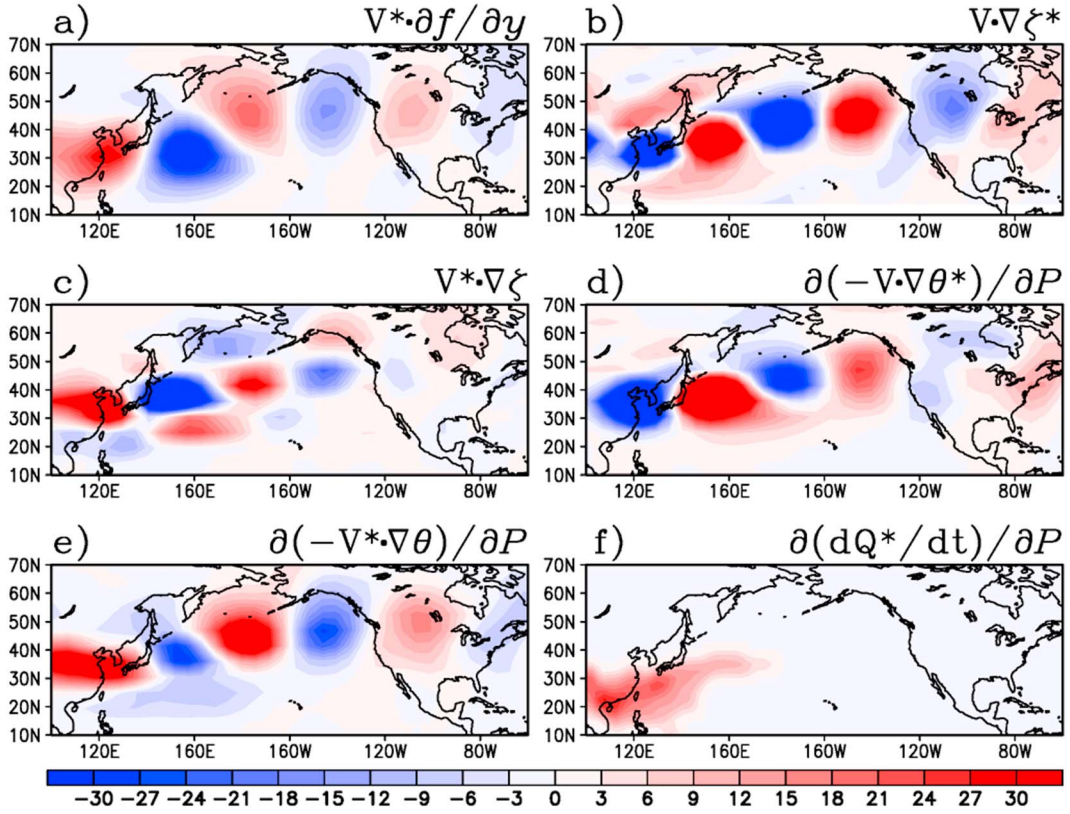

Figure 7. Spatial structure of 200-hPa geopotential height tendency forcing terms for the East Asian Monsoon teleconnection pattern. (a) Planetary vorticity advection by the anomalous wind, (b) anomalous vorticity advection by the mean wind, (c) mean vorticity advection by the anomalous wind, (d) differential anomalous potential temperature advection by the mean wind, (e) differential mean potential temperature advection by the anomalous wind, and (f) differential diabatic heating applied as heating rate forcing. Positive (red) shading indicates geopotential height rise.

volume, and $h = \frac{R}{p_o}\left(\frac{p_o}{p}\right)^{\frac{c_v}{c_p}}$. The equation is evaluated at pressure level $p = 200$ hPa, using $p_0 = 1{,}000$ hPa as the reference pressure. The overbar denotes the mean (i.e., background state taken as the summer or JJA season) used here to linearize the LBM, whereas the star denotes the LBM anomalous response to the applied diabatic heating rate.

$$x \sim -\left(\nabla^2 + f^2\frac{\partial}{\partial p}\frac{1}{\sigma}\frac{\partial}{\partial p}\right)x$$
$$= f_0\left[\beta v^* + \overline{v}\cdot\nabla\zeta^* + v^*\cdot\nabla\overline{\zeta}\right] - {f_0}^2\frac{\partial}{\partial p}\left[\frac{h}{\sigma}\left(\overline{v}\cdot\nabla\theta^* + v^*\cdot\nabla\theta\right)\right] + \frac{{f_0}^2 R}{c_p}\frac{\partial}{\partial p}\left[\frac{1}{\sigma p}\frac{dQ^*}{dt}\right]$$
(1) (2) (3) (4) (5) (6)

Since the LBM response is steady state, the left-hand side is equal to zero, and therefore, the six terms on the right-hand side should balance each other. These are as follows: (1) planetary vorticity advection by the anomalous wind, (2) anomalous vorticity advection by the mean wind, (3) mean vorticity advection by the anomalous wind, (4) differential anomalous potential temperature advection by the mean wind, (5) differential mean potential temperature advection by the anomalous wind, and (6) differential diabatic heating applied as heating rate forcing (Figures 5b and 5d).

The budget equation above is used to quantify the relative contribution of each term to the stationary teleconnection pattern in Figure 6a for JJA over the forcing region (i.e., EAM) and over the Great Plains of the United States (i.e., over the heat wave region). These six forcing terms from the budget equation are shown in Figure 7 where positive contours indicate geopotential height increase. In general, the planetary vorticity advection by the anomalous wind (Figure 7a) and the differential mean potential temperature

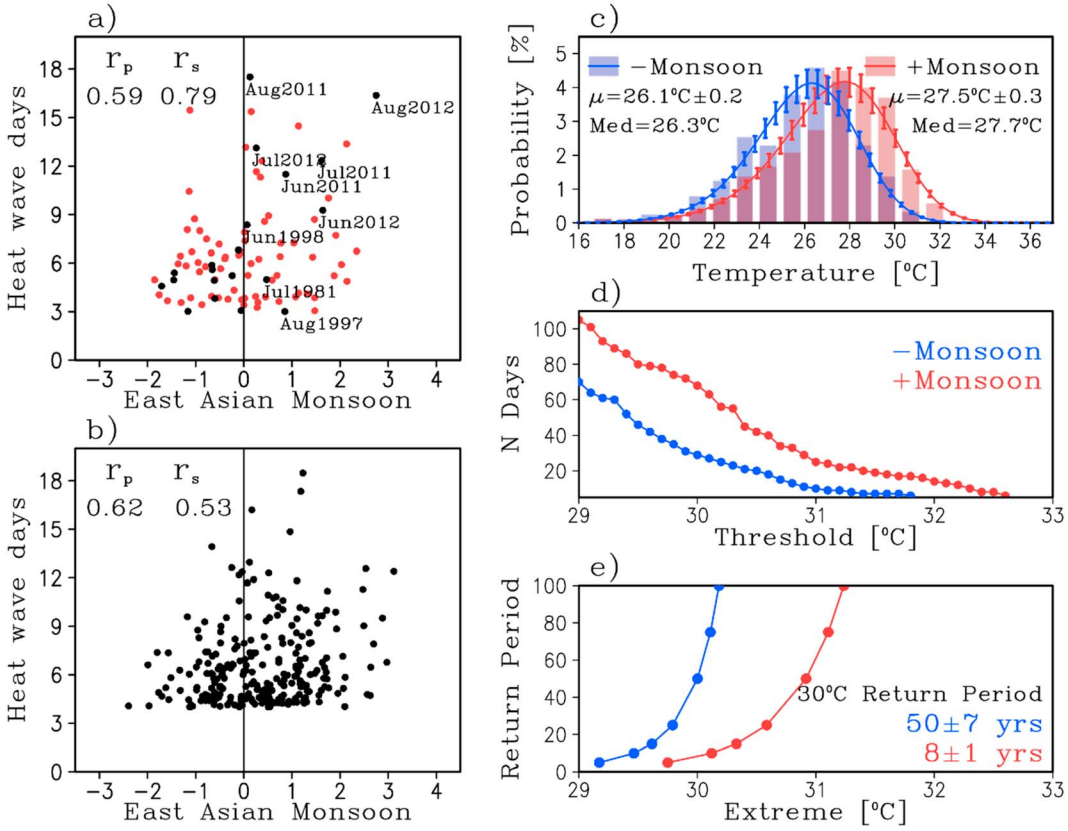

Figure 8. (a) Scatter diagram of the observed East Asian Monsoon (EAM) index versus the observed number of heat wave days over the Great Plains with the month and year of the strong events highlighted. The observed EAM index is based on precipitation (black, from 1979 to 2016) and a reconstructed index based on 850-hPa vorticity (red, from 1900 to 1978). (b) Same as (a) but for the Community Earth System Model preindustrial simulation. (c) Probability density function of June-July-August summer surface air temperature over the Great Plains for those summers with strong (red) and weak (blue) EAM. The distribution is modeled as an stochastically generated skewed distribution and the uncertainty estimates obtained from the Markov model at a 95% confidence level. (d) Histogram of the number of days exceeding a high-threshold during summer days of strong (red) and weak (blue) EAM. (e) Return period in years as a function of high-extremes obtained by a Pareto distribution. The return period for the 30 °C is specified for strong (red) and weak (blue) EAM summers.

advection by the anomalous wind (Figure 7e) are in phase and support westward propagation of the stationary pattern shown in Figure 6 as inferred from the height tendencies. However, these two terms are generally balanced by anomalous vorticity advection by the mean wind (Figure 7b) and by differential anomalous potential temperature advection by the mean wind (Figure 7d), and these supports eastward propagation of the stationary pattern in Figure 6. Mean vorticity advection by the anomalous wind (Figure 7c) is only important over the western half of the domain, mostly due to the strong background flow there. As expected by quasigeostrophic theory, the height tendency response to heating prescribed in the LBM is positive at 200 hPa over the heating region associated with the EAM (Figure 7f); thus, the geopotential height rises above the heating source. It can be seen that the differential diabatic heating (Figure 7e) has a similar spatial pattern as the EAM heating rate prescribed to the LBM as forcing (Figure 5). The heating anomaly over the EAM leads to a geopotential height rises above the heating source. This positive height anomaly excites a wave train extending eastward in the relative strong background westerly wind (Figure 5b), thus leading to anticyclonic circulation patterns downstream of the heating source (Figure 6). Note that we have excluded the contribution of the eddy terms (i.e., product of star * terms) as their influence on the height tendency are an order of magnitude smaller compared to the other terms in the equation (not shown).

5. Extreme Value Analysis

The likelihood of Great Plains heat waves as a function of the EAM state is assessed by a scatter diagram of the EAM index and the number of heat wave days (Figures 8a and 8b). Note that most of the extreme cases of

persistent heat extremes occur during those summers with a more active EAM in both observational estimates (Figure 8a) and CESM (Figure 8b). We assess changes in the probability density function (PDF) of summer temperature extremes associated with the EAM by modeling the PDF as a stochastically generated skewed (SGS) distribution (Sardeshmukh et al., 2015) and applied to summer temperatures (Lopez et al., 2018). For this, we compute the PDF for those summers with strong and weak EAM separately. Strong (weak) EAM is defined when the EAM index is larger (smaller) than one (minus one) standard deviation.

Figure 8c shows the SGS PDF of JJA daily-mean surface temperature over the Great Plains heat wave region for the 1,100-year preindustrial simulation of CESM conditioned by the state of the EAM. Performing this analysis with purely observations is challenging due to the short observational period for precipitation over the EAM region. CESM accurately reproduces the negative skewness of the observed temperature PDF, as was shown in Lopez et al. (2018). Note that there is a significant shift to warmer temperatures over the Great Plains during those summers when the EAM precipitation activity is stronger, with mean JJA temperatures of 27.5°C compared to 26.1°C for weak EAM summers. This difference is significantly larger than those expected by pure random error at a 95% confidence interval. Random error is quantified here by the use of a Markov model with parameters consistent with the SGS distribution following Lopez et al. (2018).

The SGS distribution is a useful tool in the analysis of changes in temperature conditioned by the state of the EAM. But, little can be diagnosed about the extremes because the SGS and other commonly used distributions cannot model the behavior of extremes (i.e., the tail regions). For this reason, we rely on extreme value theory by modeling the right-tail (extreme high temperatures) of the temperature over the Great Plains. The Generalized Pareto distribution (Coles, 2001) is used as a model of excess over a high threshold by looking at JJA daily mean air temperature greater than a fixed threshold, typically greater than the 95th percentile. In order to avoid temporal correlation between supposedly independent values for a given location (e.g., consecutive days exceeding a threshold but being part of the same phenomena), we cluster the excess over the threshold by identifying independent clusters. Therefore, each cluster is separated from the rest by at least 8 days, which guarantees that each extreme is synoptically independent.

There is a marked increase in the frequency of extreme temperature events over a high threshold for those summers in which the EAM is strong versus those summers in which it is weak (Figures 8d and 8e). The return period as a function of high-threshold extreme events are also quantified by the Pareto distribution and shown in Figure 8e. Note that these high-temperature extremes occur more often during those summers with more active EAM. For example, the 30 °C event has a return period of 50 years during weak EAM, in contrast to an 8-year occurrence during strong EAM. These results are consistent with the circulation anomalies shown in Figure 3 for observational estimates and CESM and in Figure 6 for the LBM experiment. The 2011 and 2012 observed summer heat waves occurred during anomalous positive EAM, as shown by the positive precipitation anomaly over the southern tip of Japan and the Korean peninsula in June, which then propagated northward later in the summer (Figure 9). It can be observed that the Great Plains were anomalously dry during those two summers, consistent with the anticyclonic circulation pattern and the occurrence of extreme heat waves there. The northward propagation of the precipitation pattern is common with the EAM, followed by an abrupt weakening in the late summer, as described in Sample and Xie (2009). The northward seasonal migration of the rainband is associated with the northward shift of the axis of the North Pacific Subtropical High and a deepening of a sea level pressure trough on the western flank of the subtropical high. This is also consistent with the northward migration and weakening of the background flow as well as the teleconnection pattern as one progresses from early to late summer.

6. Discussion

This study investigates the potential drivers of heat waves over the Great Plains of the United States, motivated by the very extreme 2011 and 2012 summer heat waves that caused hundreds of fatalities and vast economic losses. Using observational estimates, a state-of-the-art coupled general circulation model simulation, and a simple atmospheric linear baroclinic model experiment, we show that variations of the EAM modulates the occurrence and frequency of heat waves over the Great Plains of the United States. The atmospheric teleconnection mechanism outlined here begins with the diabatic heating associated with deep convection and precipitation over the EAM region. This deep convection occurs under the climatological right-entrance region of the JJA jet streak circulation, which supports the rising motion in the middle troposphere. The

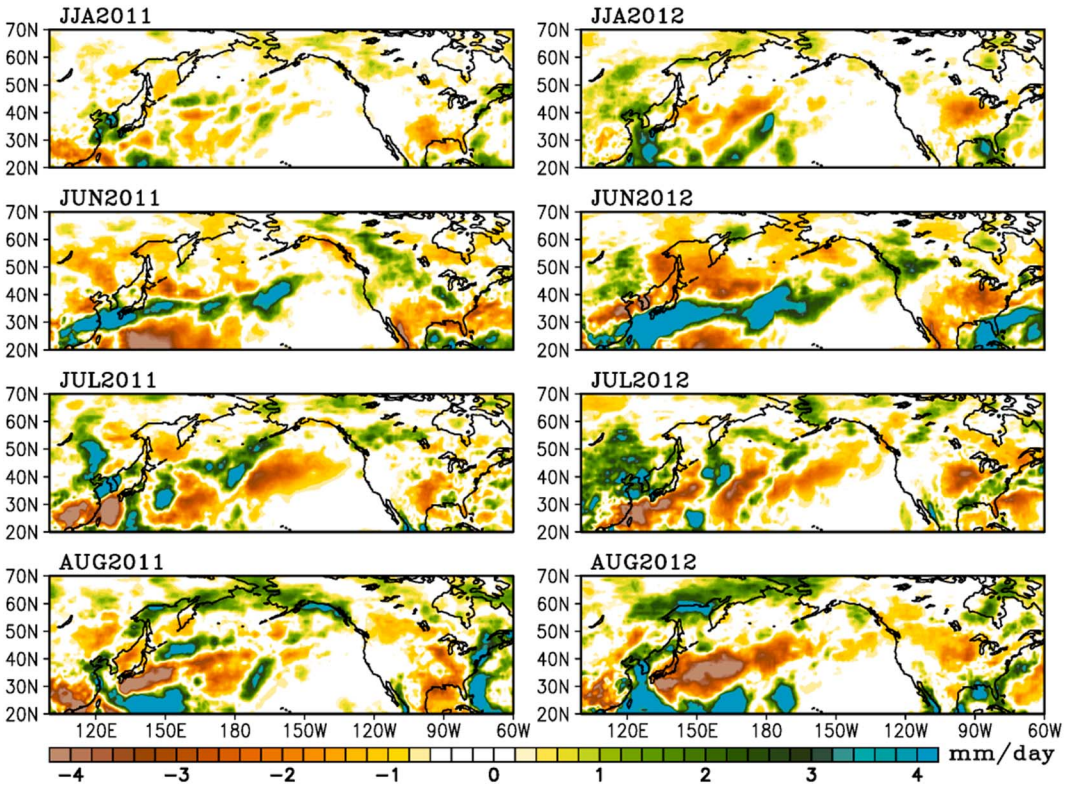

Figure 9. Interannual precipitation anomaly during the boreal summers of 2011 (left column) and 2012 (right column). Note the anomalous positive East Asian Monsoon precipitation as it marches poleward from June to August depicting a more active than normal monsoon precipitation.

midlevel positive diabatic heating induces an upper-level ridge (i.e., anticyclone over the EAM), and the associated anomaly excites a wave-train that extends east in the relative strong westerlies, eventually reaching the Great Plains of the United States. This eastward propagation was described by quantifying the stationary wave energy flux associated with the circulation anomaly at 200 hPa as well as by analyzing a budget equation of geopotential height tendency. An anticyclonic circulation pattern over the Great Plains serves as a blocking pattern for transient storms and is supportive of persistent drought and clear sky conditions, promoting high summer temperatures and heat waves. These upper-level anticyclonic patterns are often long-lived and supported by strong static stability, diabatic cooling due to radiation loss at upper levels, and near-surface diabatic heating due to sensible heat flux at low levels.

The Great Plains is in a transitional hydrological regime in which soil moisture is a limiting constraint on evapotranspiration and latent heating, influencing climate variability through coupling and feedbacks between the atmosphere and land (Koster et al., 2006; Seneviratne et al., 2010). For example, a reduction in precipitation in association with a remotely forced upper-level anticyclone leads to a reduction in soil moisture and an increased solar radiative heat flux. The enhanced solar radiative heat flux and soil drying promotes more sensible heat flux than latent heat flux, thus increasing surface air temperature. Consistent with this, Lopez et al. (2018) found that uncertainty in future projections of heat waves over the Great Plains is caused by the uncertainty in the land response to a projected increase in the variability of moisture flux, precipitation, and soil moisture there.

In this study, the EAM variability is shown to be a potential predictor of high-impact Great Plains heat waves. Given this, it should be noted that climate models have difficulties in simulating global monsoon precipitation, although there have been some recent improvements. For example, Sperber et al. (2013) analyzed the boreal summer Asian monsoon system in the Coupled Model Intercomparison Project phases 5 and 3 (i.e., CMIP5 and CMIP3) models. They found an improvement in the simulation of monsoon circulation and precipitation from CMIP3 to CMIP5 models, where the later models can reproduce some aspects (e.g., time-mean, annual cycle, intraseasonal, and interannual variability) of the monsoon. In addition, Lopez

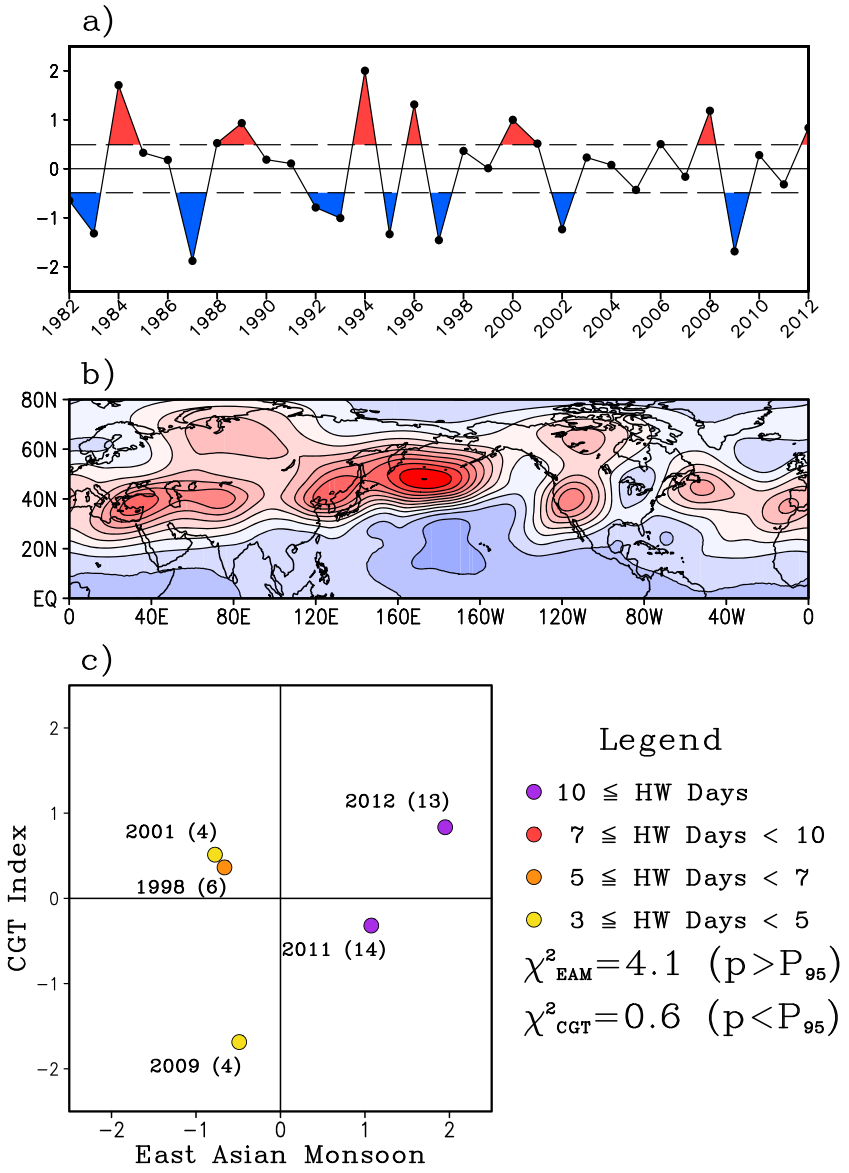

Figure 10. (a) Observed normalized circumglobal teleconnection (CGT) index and (b) the spatial map associated with the CGT index as defined by an empirical orthogonal function analysis of June-July-August 200-hPa geopotential height variability. (c) Scatter diagram of the number of heat wave (HW) days over the Great Plains with respect to the East Asian Monsoon (EAM) index (x axis) and the CGT index (y axis). Heat wave days are color coded as in the legend with their respective year shown as well as the number of days (parenthesis). χ^2 values given for the composites of heat wave days for positive and negative EAM and CGT indices.

et al. (2016) showed that the CESM model used here accurately reproduces the mean seasonal cycle for all monsoon regions, although with considerably weaker precipitation during the active phase.

Our results show a logical analysis depicting a modulation in probabilities of Great Plains heat events through remote teleconnections forced during strong EAM years. Although the analysis based on the coupled model and on the LBM may indicate a "causality," there could still be a possibility that both (enhanced EAM and number of heat waves) may be part of a single global circulation feature during summer (e.g., the circumglobal teleconnection pattern [CGT] of Branstator, 2002). The CGT is a wavenumber-5 teleconnection pattern of the Northern Hemisphere midlatitudes, which modulates temperature and precipitation over Asia, Europe, and North America. Ding and Wang (2005) showed that the CGT is maintained by the interaction of the Indian summer monsoon heating and global wave train along the storm track.

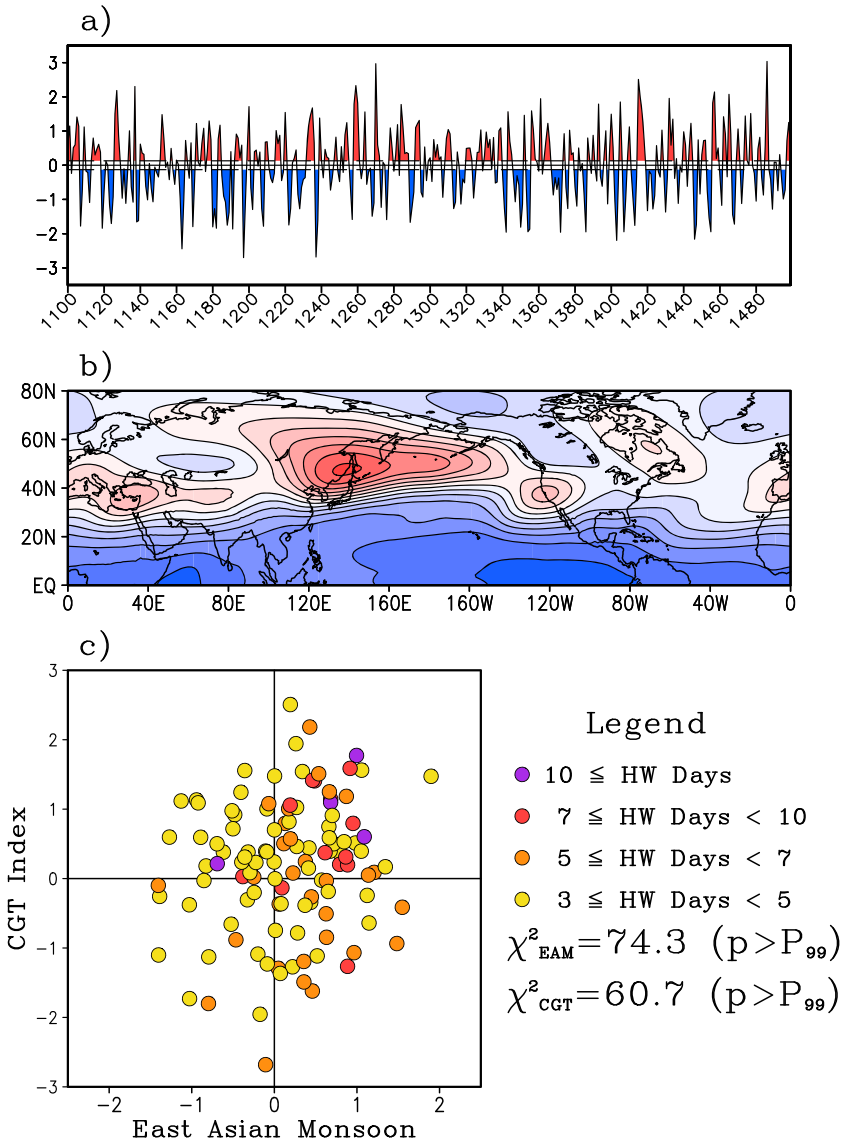

Figure 11. Same as Figure 10 but for the Community Earth System Model.

Here we show that the EAM and the CGT are uncorrelated, and their teleconnection patterns are distinct (Figures 10 and 11). The recent 2011 (2012) Great Plains heat wave events occurred during a positive (negative) CGT index, whereas the EAM was strongly positive for both years (Figure 10). While analysis of the CESM simulation shows that the number of heat waves increases for those summers when both the EAM and the CGT are positive, the EAM dominates their occurrence (Figure 11). It is also possible that the CGT is a combination of different teleconnection patterns driven by different heating over different regions, but more analysis is required to discern the CGT influence on heat waves and is beyond the scope of this study.

Finally, these results provide a useful basis in order to understand potential mechanisms of drivers of heat waves with the aim at improving their predictions. However, there are still many open questions. For example, is there any skill in predicting EAM precipitation and associated teleconnection patterns with useful lead time, which can help forewarn the occurrence of heat waves over the Great Plains (i.e., subseasonal-to-seasonal predictions)? Also, is the mechanism outlined in this study subseasonally dependent (i.e., more robust during early or late summer) given the significant meridional shift of the westerly jet over East Asia, thus potentially altering teleconnections as suggested by the LBM experiment?

The EAM tends to be above (below) normal in the boreal summers following a mature El Niño (La Niña) phase (Wang et al., 2001). A mechanism describing the ENSO influence on the EAM was presented in Wang et al. (2001). This mechanism involves the strengthening of a low-level anticyclonic circulation over the Philippine Sea (namely, the Western Pacific Subtropical High) during the El Niño phase, which is then maintained through the subsequent summer by air-sea feedbacks. This subtropical high produces southwesterly wind on its western flank, enhancing the low-level warm and moist air advection, strengthening the EAM convection (Wu et al., 2003; Zhang et al., 2017). These studies suggest the possibility for prediction skill of the EAM teleconnection pattern beyond the typical weather timescale. With regards to potential longer-term predictability, Lopez et al. (2016) demonstrated a decadal link between the Atlantic Ocean meridional overturning circulation and variations in the global monsoon, including the EAM. Could the mechanism outlined here be extended to assess decadal changes in heat wave occurrence?

Predictability assessment of the teleconnection pattern and heat waves presented here is planned for the future using the North America by making use of the National Multimodel Ensemble forecast system (Kirtman et al., 2014).

Acknowledgments
We would like to acknowledge the anonymous reviewers, which their comments helped improve the quality of this manuscript. We would also like to acknowledge Ghassan Alaka (NOAA/AOML) and Elizabeth Johns (NOAA/AOML) for their comments and suggestions. This research was carried out in part under the auspices of the Cooperative Institute for Marine and Atmospheric Studies, a cooperative institute of the University of Miami and the National Oceanic and Atmospheric Administration (NOAA), cooperative agreement NA10OAR4320143. This work was funded by NOAA's Atlantic Oceanographic and Meteorological Laboratory and by the NOAA Climate Program Office CVP program (GC16-208). The ERA-20C reanalysis was provided by ECMWF at https://www.ecmwf.int/en/forecasts/datasets/reanalysis-datasets/era-20c. The JRA-25 reanalysis was obtained from the Research Data Archive at NCAR: https://rda.ucar.edu/datasets/ds625.0/. The CESM model simulation was obtained from the Climate Data Gateway at NCAR: https://www.earthsystemgrid.org. The LBM model code and documentation were obtained from http://ccsr.aori.u-tokyo.ac.jp/~lbm/sub/lbm.html.

References

Atlas, R., Wolfson, N., & Terry, J. (1993). The effect of SST and soil moisture anomalies on GLA model simulations of the 1988 U.S. summer drought. *Journal of Climate*, *6*(11), 2034–2048. https://doi.org/10.1175/1520-0442(1993)006<2034:TEOSAS>2.0.CO;2

Bluestein, H. B. (1993). Synoptic-dynamic meteorology in midlatitudes. Volume II. Observations and theory of weather systems.

Branstator, G. (2002). Circumglobal teleconnections, the jet stream waveguide, and the North Atlantic Oscillation. *Journal of Climate*, *15*(14), 1893–1910. https://doi.org/10.1175/1520-0442(2002)015<1893:CTTJSW>2.0.CO;2

Coles, S. (2001). *An Introduction to Statistical Modeling of Extreme Values*. London: Springer. https://doi.org/10.1007/978-1-4471-3675-0

Ding, Q., & Wang, B. (2005). Circumglobal teleconnection in the Northern Hemisphere summer. *Journal of Climate*, *18*(17), 3483–3505. https://doi.org/10.1175/JCLI3473.1

Hoerling, M., Eischeid, J., Kumar, A., Leung, R., Mariotti, A., Mo, K., et al. (2014). Causes and predictability of the 2012 Great Plains drought. *Bulletin of the American Meteorological Society*, *95*(2), 269–282. https://doi.org/10.1175/BAMS-D-13-00055.1

Hoskins, B. J., & Karoly, D. J. (1981). The steady linear response of a spherical atmosphere to thermal and orographic forcing. *Journal of the Atmospheric Sciences*, *38*(6), 1179–1196.

Huffman, G. J., Adler, R. F., Arkin, P., Chang, A., Ferraro, R., Gruber, A., et al. (1997). The Global Precipitation Climatology Project (GPCP) combined precipitation dataset. *Bulletin of the American Meteorological Society*, *78*(1), 5–20. https://doi.org/10.1175/1520-0477(1997)078<0005:TGPCPG>2.0.CO;2

Infanti, J. M., & Kirtman, B. P. (2016). North American rainfall and temperature prediction response to the diversity of ENSO. *Climate Dynamics*, *46*, 3007–3023. https://doi.org/10.1007/s00382-015-27490

Kam, J., Sheffield, J., & Wood, E. F. (2014). Changes in drought risk over the contiguous United States (1901–2012): the influence of the Pacific and Atlantic Oceans. *Geophysical Research Letters*, *41*, 5897–5903. https://doi.org/10.1002/2014GL060973

Kay, J., Deser, C., Phillips, A., Mai, A., Hannay, C., & Strand, G. (2015). Arblaster, The Community Earth System Model (CESM) Large Ensemble Project: A community resource for studying climate change in the presence of internal climate variability. *Bulletin of the American Meteorological Society*, *96*(8), 1333–1349. https://doi.org/10.1175/BAMS-D-13-00255.1

Kirtman, B. P., Paolino, D. A., Kinter, J. L. III, & Straus, D. M. (2001). Impact of tropical subseasonal SST variability on seasonal mean climate. *Monthly Weather Review*, *129*(4), 853–868. https://doi.org/10.1175/1520-0493(2001)129<0853:IOTSSV>2.0.CO;2

Kirtman, B. P., Min, D., Infanti, J. M., Kinter, J. L. III, Paolino, D. A., Zhang, Q., et al. (2014). The North American multimodel ensemble: Phase-1 seasonal-to-interannual prediction; Phase-2 toward developing intraseasonal prediction. *Bulletin of the American Meteorological Society*, *95*(4), 585–601. https://doi.org/10.1175/BAMS-D-12-00050.1

Kodama, Y.-M. (1992). Large-scale common features of subtropical precipitation zones (the Baiu frontal zone, the SPCZ, and the SACZ). Part I: Characteristics of subtropical frontal zones. *Journal of the Meteorological Society of Japan*, *70*, 813–836.

Koster, R. D., Guo, Z. C., Dirmeyer, P. A., Bonan, G., Chan, E., Cox, P., et al. (2006). GLACE: The Global Land–Atmosphere Coupling Experiment. Part I: Overview. *Journal of Hydrometeorology*, *7*, 590–610.

Lee, S.-K., Lopez, H., Chung, E.-S., DiNezio, P., Yeh, S.-W., & Wittenberg, A. T. (2018). On the fragile relationship between El Niño and California rainfall. *Geophysical Research Letters*, *45*, 907–915. https://doi.org/10.1002/2017GL076197

Lee, S. K., Wang, C., & Mapes, B. E. (2009). A simple atmospheric model of the local and teleconnection responses to tropical heating anomalies. *Journal of Climate*, *22*(2), 272–284. https://doi.org/10.1175/2008JCLI2303.1

Lin, Y. H., Hipps, L. E., Wang, S. Y. S., & Yoon, J. H. (2017). Empirical and modeling analyses of the circulation influences on California precipitation deficits. *Atmospheric Science Letters*, *18*(1), 19–28. https://doi.org/10.1002/asl.719

Lopez, H., Dong, S., Lee, S. -K., & Goni, G. (2016). Decadal modulations of interhemispheric global atmospheric circulations and monsoons by the south Atlantic meridional overturning circulation. *Journal of Climate*, *29*(5), 1831–1851. https://doi.org/10.1175/JCLI-D-15-0491.1

Lopez, H., West, R., Dong, S., Goni, G., Kirtman, B., Lee, S. K., & Atlas, R. (2018). Early emergence of anthropogenically forced heat waves in the western United States and Great Lakes. *Nature Climate Change*, 1.

Meehl, G. A., & Tebaldi, C. (2004). More intense, more frequent, and longer lasting heat waves in the 21st century. *Science*, *305*(5686), 994–997.

Namias, J., & Clapp, P. F. (1949). Confluence theory of the high tropospheric jet stream. *Journal of Meteorology*, *6*(5), 330–336.

Onogi, K., Tsutsui, J., Koide, H., Sakamoto, M., Kobayashi, S., Hatsushika, H., et al. (2007). The JRA-25 reanalysis. *Journal of the Meteorological Society of Japan*, *85*(3), 369–432. https://doi.org/10.2151/jmsj.85.369

Palmer, T. N. (2013). Climate extremes and the role of dynamics. *Proceedings of the National Academy of Sciences of the United States of America*, *110*(14), 5281–5282. https://doi.org/10.1073/pnas.1303295110

Petoukhov, V., Rahmstorf, S., Petri, S., & Schellnhuber, H. J. (2013). Quasiresonant amplification of planetary waves and recent Northern Hemisphere weather extremes. *Proceedings of the National Academy of Sciences of the United States of America*, *110*(14), 5336–5341. https://doi.org/10.1073/pnas.1222000110

Piao, L., Fu, Z., & Yuan, N. (2016). "Intrinsic" correlations and their temporal evolutions between winter-time PNA/EPW and winter drought in the west United States. *Scientific Reports*, *6*(1), 19958. https://doi.org/10.1038/srep19958

Plumb, R. A. (1985). On the three-dimensional propagation of stationary waves. *Journal of the Atmospheric Sciences*, *42*(3), 217–229. https://doi.org/10.1175/1520-0469(1985)042<0217:OTTDPO>2.0.CO;2

Poli, P., Hersbach, H., Dee, D. P., Berrisford, P., Simmons, A. J., Vitart, F., et al. (2016). ERA-20C: An atmospheric reanalysis of the twentieth century. *Journal of Climate*, *29*(11), 4083–4097. https://doi.org/10.1175/JCLI-D-15-0556.1

Sampe, T., & Xie, S. P. (2010). Large-scale dynamics of the Meiyu-Baiu rainband: Environmental forcing by the westerly jet. *Journal of Climate*, *23*(1), 113–134. https://doi.org/10.1175/2009JCLI3128.1

Sardeshmukh, D. P., Compo, G. P., & Penland, C. (2015). Need for caution in interpreting extreme weather statistics. *Journal of Climate*, *28*(23), 9166–9187. https://doi.org/10.1175/JCLI-D-15-0020.1

Sardeshmukh, P. D., & Hoskins, B. J. (1988). The generation of global rotational flow by steady idealized tropical divergence. *Journal of the Atmospheric Sciences*, *45*, 1228–1251.

Schneider, T., Bischoff, T., & Plotka, H. (2014). Physics of changes in synoptic midlatitude temperature variability. *Journal of Climate*, *28*, 2312–2331. https://doi.org/10.1175/JCLI-D-14-00632.1

Screen, J. A. (2014). Arctic amplification decreases temperature variance in northern mid- to high-latitudes. *Nature Climate Change*, *4*(7), 577–582. https://doi.org/10.1038/nclimate2268

Seager, R., Goddard, L., Nakamura, J., Henderson, N., & Lee, D. E. (2014). Dynamical causes of the 2010/11 Texas–northern Mexico drought. *Journal of Hydrometeorology*, *15*(1), 39–68. https://doi.org/10.1175/JHM-D-13-024.1

Seneviratne, S. I., Corti, T., Davin, E. L., Hirschi, M., Jaeger, E. B., Lehner, I., et al. (2010). Investigating soil moisture–climate interactions in a changing climate: A review. *Earth-Science Reviews*, *99*(3-4), 125–161. https://doi.org/10.1016/j.earscirev.2010.02.004

Shepherd, T. G. (2014). Atmospheric circulation as a source of uncertainty in climate change projections. *Nature Geoscience*, *7*(10), 703–708. https://doi.org/10.1038/ngeo2253

Sperber, K. R., Annamalai, H., Kang, I.-S., Kitoh, A., Moise, A., Turner, A., et al. (2013). The Asian summer monsoon: An intercomparison of CMIP5 vs. CMIP3 simulations of the late 20th century. *Climate Dynamics*, *41*(9-10), 2711–2744. https://doi.org/10.1007/s00382-012-1607-6

Sutton, R. T., & Hodson, D. L. (2005). Atlantic Ocean forcing of North American and European summer climate. *Science*, *309*(5731), 115–118.

Teng, H., Branstator, G., Meehl, G. A., & Washington, W. M. (2016). Projected intensification of subseasonal temperature variability and heat waves in the Great Plains. *Geophysical Research Letters*, *43*, 2165–2173. https://doi.org/10.1002/2015GL067574

Teng, H., Branstator, G., Wang, H., Meehl, G. A., & Washington, W. M. (2013). Probability of US heat waves affected by a subseasonal planetary wave pattern. *Nature Geoscience*, *6*(12), 1056

Wang, B., Wu, R., & Lau, K. M. (2001). Interannual variability of the Asian summer monsoon: Contrasts between the Indian and the western North Pacific–East Asian monsoons. *Journal of Climate*, *14*(20), 4073–4090. https://doi.org/10.1175/1520-0442(2001)014<4073:IVOTAS>2.0.CO;2

Wang, B., Wu, Z., Li, J., Liu, J., Chang, C.-P., Ding, Y., & Wu, G. (2008). How to measure the strength of the East Asian summer monsoon. *Journal of Climate*, *21*(17), 4449–4463. https://doi.org/10.1175/2008JCLI2183.1

Wang, H., Schubert, S., Koster, R., Ham, Y. G., & Suarez, M. (2014). On the role of SST forcing in the 2011 and 2012 extreme US heat and drought: A study in contrasts. *Journal of Hydrometeorology*, *15*(3), 1255–1273. https://doi.org/10.1175/JHM-D-13-069.1

Wang, H., Wang, B., Huang, F., Ding, Q., & Lee, J. Y. (2012). Interdecadal change of the boreal summer circumglobal teleconnection (1958–2010). *Geophysical Research Letters*, *39*, L12704. https://doi.org/10.1029/2012GL052371

Watanabe, M., & Kimoto, M. (2000). Tropical-extratropical connection in the Atlantic atmosphere-ocean variability. *Geophysical Research Letters*, *26*(15), 2247–2250. https://doi.org/10.1029/1999GL900350

Wu, R., Hu, Z. Z., & Kirtman, B. P. (2003). Evolution of ENSO-related rainfall anomalies in East Asia. *Journal of Climate*, *16*(22), 3742–3758. https://doi.org/10.1175/1520-0442(2003)016<3742:EOERAI>2.0.CO;2

Zhang, R., Min, Q., & Su, J. (2017). Impact of El Niño on atmospheric circulations over East Asia and rainfall in China: Role of the anomalous western North Pacific anticyclone. *Science China Earth Sciences*, *60*(6), 1124–1132. https://doi.org/10.1007/s11430-016-9026-x

Zhu, Z., & Li, T. (2016). A new paradigm for continental U.S. summer rainfall variability: Asia-North America teleconnection. J. *Climate*, *29*(20), 7313–7327. https://doi.org/10.1175/JCLI-D-16-0137.1

Zhu, Z., & Li, T. (2018). Amplified contiguous United States summer rainfall variability induced by East Asian Monsoon interdecadal change. *Climate Dynamics*, *50*(9-10), 3523–3536. https://doi.org/10.1007/s00382-017-3821-8